Appendix F39

Woodside 2014

First Order Analytical Estimates of Scott Reef Subsidence as a result of Reservoir Compaction in the Torosa Field, Browse Basin

BROWSE FLNG DEVELOPMENT
Draft Environmental Impact Statement

EPBC 2013/7079
November 2014

First Order Analytical Estimates of Scott Reef Subsidence as a result of Reservoir Compaction in the Torosa Field, Browse Basin.

Browse Reservoir Development

Date: [24/02/14]

1 Executive Summary

Document purpose: Provide an estimate of reservoir compaction and associated surface subsidence due to the planned production of the Torosa gas reservoir. Furthermore, describe the analytical estimate methodology and results with reference to the predicted surface subsidence at the overlying reef system of Scott Reef.

The Torosa gas accumulation spans an area approximately 50 km by 15 km within a layer of rock up to 500 m thick and over 4000 m below sea level. A significant part of this reservoir layer lies beneath Scott Reef. Production of hydrocarbons from the reservoir is expected over a period of 40 years. The gross reservoir interval contains three distinct reservoir units (referred to as J18, J22 and J28.3).

Minor reservoir compaction is expected to occur as the pore pressure within the reservoir rock is decreased due to production. The rock matrix compacts as it takes up the stress previously supported by the pore fluid – resulting in a thinning of the reservoir. The amount of thinning depends on the thickness of the depleting reservoir rock, the uniaxial strain compaction coefficient of the rock and the pore pressure change. Surface subsidence is the surface expression of, and occurs in response to, reservoir compaction.

Reservoir compaction and surface subsidence estimates for the Torosa reservoir and the overlying reef complex were obtained by summing the compaction and subsidence from the three reservoir units (J18, J22 and J28). Subsequent to an initial prediction based on a 2012 reservoir model, subsidence predications were updated based on a 2013 reservoir model. Overall reef subsidence (updated 2013 model prediction) using the Geertsma method is estimated to be in the range of 2.58 and 8.93 cm over the life of the field with a mid-case or expected subsidence of 5.45 cm.

The reservoir compaction and surface subsidence estimates were derived from the following laboratory and modelling studies:

- Laboratory-based tests were undertaken on core samples of the reservoir units from the Torosa-1 and Torosa-6 boreholes. In addition, laboratory-based tests on Calliance reservoir cores were also used in the model. The results of these tests indicate that the rocks are relatively strong, and plot within the well-consolidated region of porosity-compaction coefficient space. This observation is consistent with the depth of burial and temperature of the reservoir rocks. As such, the reservoir compaction response to pore pressure depletion (and subsequent surface subsidence) is expected to be relatively small in comparison to other fields with weaker, more compressible reservoir rocks.

- Reservoir compaction and surface subsidence were estimated using published analytical techniques (Geertsma, 1973 & Bruno 1992). These methods assume simplistic disc-shaped reservoir geometry, and were developed for onshore fields with shallower reservoir depths than in the Torosa Field. However, use of such analytical methods is standard industry practice to obtain first-order estimates of reservoir compaction and surface subsidence.

- The inputs for the Torosa compaction and Scott Reef subsidence study were taken from reservoir modelling (i.e. radius of reservoir, pore pressure change, net reservoir height, and porosity), and a series of laboratory test results (Poisson's ratio and uniaxial strain compaction). A uniform probability function was applied to each variable to describe uncertainty except reservoir radius and depth. Variation in reservoir radius and reservoir depth would not significantly alter the subsidence estimates.

A high degree of conservatism was implicit in the interpretation of analytical results and modelling owing to the recognised uncertainties with respect to the methods used and core input data relating to the amount of production depletion and uniaxial strain compaction.

Table of Contents

2 Introduction

Reservoir compaction occurs as the pore pressure within the reservoir rock is decreased due to production. The rock matrix compacts as it takes up the stress previously supported by the pore fluid – resulting in a thinning of the reservoir. The amount of thinning depends on the thickness of the depleting reservoir rock, the uniaxial strain compaction coefficient of the rock and the pore pressure change. Surface subsidence occurs in response to reservoir compaction and is dependent on the reservoir compaction, and the geometry and geomechanical properties of the overburden.
Compaction in producing reservoirs and resulting surface subsidence are well known and documented in the oil and gas industry.

Potential problems associated with reservoir compaction and surface subsidence may include:

- Platform subsidence;
- Damage down-hole equipment (e.g. casing shear);
- Reduced reservoir porosity and permeability, and;
- Environmental concerns in certain environments sensitive to minor changes in relative sea level.

The Calliance, Brecknock and Torosa Fields are aligned along a northeast trending regional high at Jurassic level (Scott Reef trend) in the Browse Basin (Figure 1). Production at the Calliance, Brecknock and Torosa Fields is expected to be associated with significant pressure depletion over production life (~40 years). Reservoir compaction and surface subsidence which may result from the expected reservoir depletion were estimated using 1D analytical techniques proposed by Geertsma (1973) and Bruno (1992).

This study presents two subsidence predictions. The first prediction is based on the reservoir model that was applied in the year 2012. The second, updated subsidence prediction is based on the updated 2013 reservoir model.

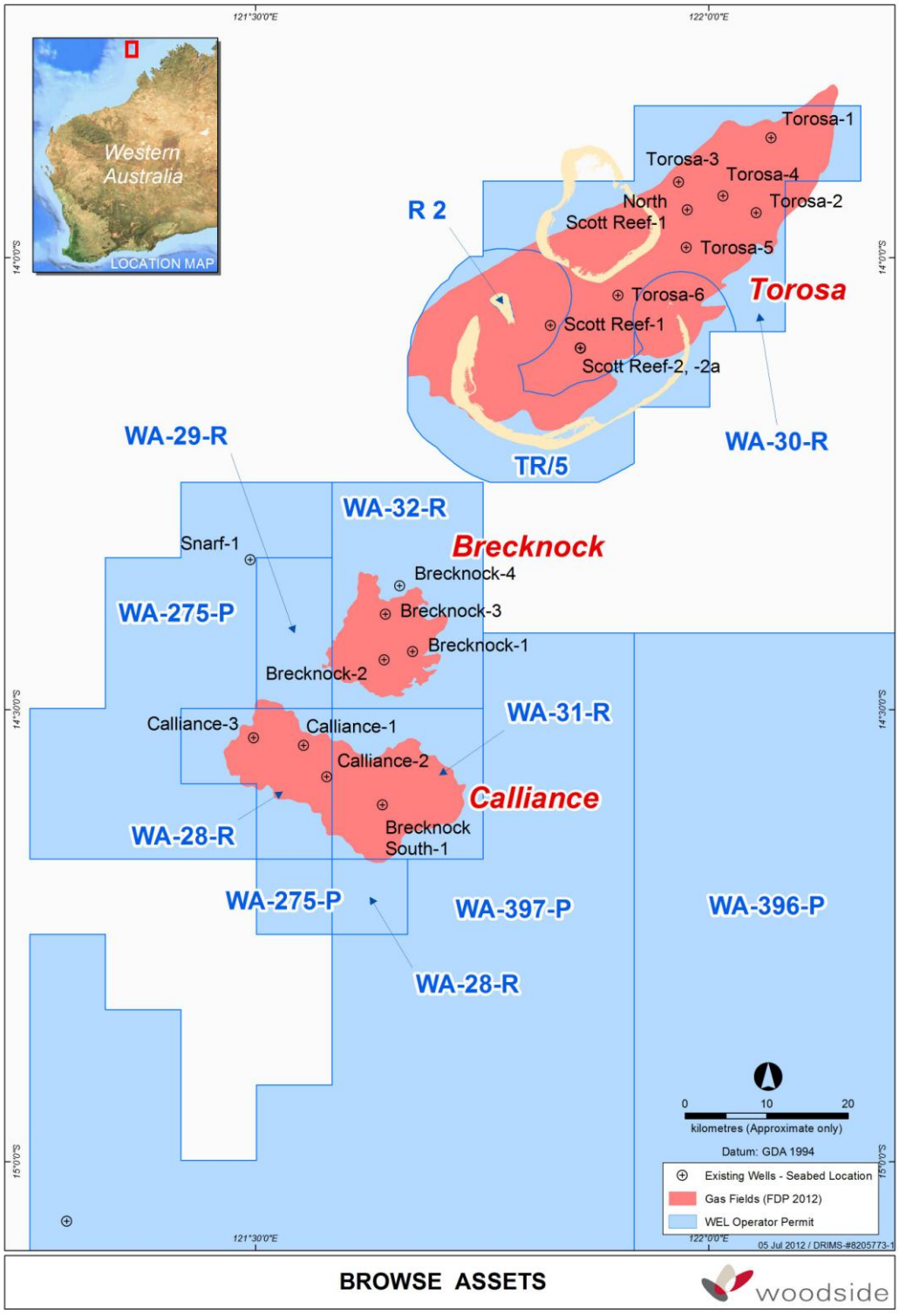

Figure 1: Browse gas accumulations.

3 Industry Example

Compaction in producing reservoirs and resulting surface subsidence are well known phenomena and documented in the oil and gas industry. Most of the documented examples of compaction and subsidence have been where significant subsidence has occurred due to production from shallow, unconsolidated reservoir rocks. A well studied and more analogous example for the Torosa field is the subsidence in the Groningen Field which has been extensively studied and measured over a 40 year production timeframe.

3.1 Groningen Field, Netherlands

The Groningen Field is an onshore gas field with a horizontal extent of ~900 km2. The gas is hosted in a sandstone reservoir at ~2825 m. Production at the Groningen gas field began in 1963. Surface monitoring using levelling techniques has been applied since the start of production (Figure 2). The surface subsidence profile is commonly referred to as the "subsidence bowl" because the profile is often bowl shaped (e.g. Figure 3). The deepest point in the Groningen "subsidence bowl" in 2003 had subsided 245 mm or 24.5 cm over the 40 year production period (Figure 2 and Figure 3). Measured surface displacements are approximately linear with time with a lag observed before the onset of subsidence at the centre of the subsidence bowl (Figure 2).

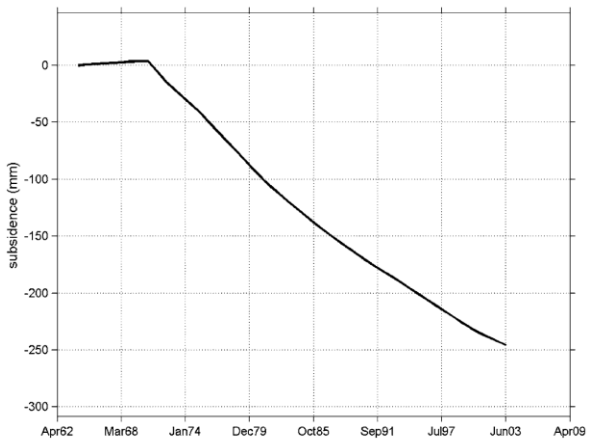

Figure 2: Subsidence since the start of gas production in the centre of the Gronigen "subsidence bowl" from levelling observations (Ketelaar, 2009). The decrease in subsidence rate from the 1970s has been attributed to a change in priority to the smaller gas fields.

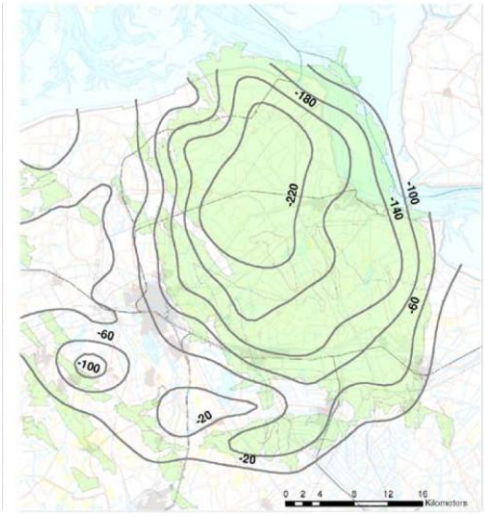

Figure 3: Subsidence since the start of production to 2003 (Ketelaar, 2009).

4 Methods and Approach to Understanding Subsidence

4.1 Introduction

Surface subsidence is the vertical change at the surface caused by the reservoir compaction. The amount of subsidence transferred to the surface by a subsurface compaction source is controlled primarily by the shape and lateral extent of the compacting zone and burial depth of the zone. Industry empirical evidence suggests that surface subsidence resulting from very shallow and laterally extensive compaction zones will tend to near zero at a lateral distance equal to approximately twice the reservoir depth.

Two approaches were undertaken to understand the potential subsidence of Scott Reef as a result of hydrocarbon extraction. The two methods that were undertaken were the Geertsma method and the Bruno method.

4.2 Geertsma Method

The first approach to predicting Scott Reef subsidence was the Geertsma (1973) method. Geertsma determined analytical equations to estimate subsidence based upon his work for Shell in sandstone and carbonate reservoirs, including the Groningen gas field in the Netherlands. This approach expresses surface subsidence ($\Delta h_{surface}$) as a function of reservoir compaction ($\Delta h_{reservoir}$), Poisson's ratio (υ) and Geertsma's look-up value (A):

$$\Delta h_{surface} = 2\ A\ (1-\upsilon)\ \Delta h_{reservoir}$$

The parameter A is related to the ratios of radius/reservoir radius and reservoir depth/reservoir radius. Reservoir compaction or change in reservoir height is given by:

$$\Delta h_{reservoir} = C_z \times h_o \times \Delta Pp$$

Where (Cz) is uniaxial strain compaction coefficient, (h_o) is initial net thickness, and (ΔPp) is change in reservoir pressure.

Horizontal surface displacement also occurs as a result of reservoir compaction. Geertsma (1973) expressed horizontal surface displacement (the distance from centre of subsidence, i.e. away from the borehole's depleting sand) using a similar equation where factor (B) is obtained from a table published by Geertsma (1973) and is related to reservoir radius and reservoir depth:

$$\Delta Surface = 2\ B\ (1-\upsilon)\ \Delta h_{reservoir}$$

4.3 Bruno Method

Bruno developed an equation for determining subsidence based largely on his work with southern California fields. The Bruno (1992) approach estimates maximum vertical subsidence (S) at the centre of the field using the following equation:

$$S = 2 \times Cz \times (1-\upsilon) \times [H - (R^2 + (D+H)^2)^{0.5} + (R^2 + D^2)^{0.5}] \times \Delta Pp$$

where

H = net reservoir thickness (m)
R = reservoir radius (m)
D = reservoir depth (meters below mud line)

Note on Bruno equation:

Original equation lists Cm as the uniaxial compaction coefficient. Cz has been substituted for Cm for consistency with other equations and tables in this report.

4.4 Input Data and Assumptions

Input parameters used in this study have been obtained from laboratory tests undertaken on core samples and wireline log data from the nine exploration and appraisal wells in the Torosa Field. Parameters have been estimated away from well control using 3D seismic data, geological modelling and dynamic reservoir simulation (Table 1).

Input parameter	Abbreviation	Source
Uniaxial strain compaction coefficient (average)	Cz	Estimated using average porosity. The porosity-compaction relationship was established using laboratory data (see **Section 5**).
Porosity (average)	ϕ	Average porosity has been used to constrain Cz – it is not used directly in the calculations. Porosity is taken from the geological model. Porosity is estimated at each well location using log-based methods calibrated to core measurements. Porosity is estimated away from well control using geostatistics within a geologically constrained framework.
Reservoir depletion	ΔPp	Average reservoir depletion is estimated from dynamic reservoir modelling which simulates production. Multiple simulations have been performed using different realisations of the geological model and with varying parameters such as aquifer strength and fault seal. Extreme high and low case predictions were obtained from a range of pressure depletions resulting from multiple model realisations.
Net reservoir thickness (average)	H	Taken from the geological model. The framework geological model is built using well and seismic data. Gross reservoir thickness is constrained at each well location, and estimated away from well control using seismic data. Net-to-gross (NTG) is estimated at each well location using log data, and constrained away from well locations using geostatistics within a geologically constrained framework. Average net reservoir thickness is obtained by multiplying NTG by gross reservoir thickness. Low, mid and high cases were used from multiple model realisations.
Reservoir radius	R	Chosen such that the area of the circle is equal to the area of the field. The area of the field is defined using well and seismic data.
Reservoir Depth	D	Reservoir depth from geological model. Constrained with well and seismic data.
Poisson's Ratio (average)	υ	Estimated at each well location by log-based methods calibrated to laboratory measurements.

Table 1: Summary of input parameters and their derivation.

The following assumptions were made when calculating subsidence:

- An arching effect was not included: The arching effect occurs when the rocks overlying the compacting reservoir support the overlying rock mass to an extent, limiting the resulting surface subsidence. Hence, the estimated subsidence values are on the conservative side;
- It is assumed that the reservoir compacts uniaxially in the vertical direction;
- The radius of the disc representing each reservoir was chosen such that the area of the disc was equal to the area of the each reservoir;
- The depleting reservoir units vary spatially such that the contribution of each unit to total reservoir compaction will vary across the field. A conservative approach was

undertaken where it was assumed that the thickest section of each of the reservoir units overlie each other, and;

- The centre of the subsidence bowl hasn't been defined. Instead, it is assumed maximum subsidence could occur everywhere within the field and in areas surrounding the field.

5 Laboratory Inputs into Subsidence Prediction (Geertsma and Bruno Methods)

5.1 Uniaxial Strain Compaction Tests

Laboratory tests were undertaken on full core samples from the different reservoir intervals of Torosa (and Calliance) to measure uniaxial strain compaction coefficient (Cz). Cz is a key input into the Geertsma and Bruno Subsidence Methods – the higher the Cz the more compaction will occur.

Standard core handling procedures were undertaken on the rig. Core barrels were cut into 4.5 m or 9 m lengths and end capped to ensure the cores did not dehydrate. Samples plugs were cut approximately 1.5 inch in diameter and 3 inches in length, where possible. The sample plugs were trimmed under brine and then ground flat and parallel in accordance with International Society of Rock Mechanics (IRSM) recommended procedures. Clays were kept stable in the rocks by using a formulated brine of equivalent or higher salinity than the formation salinity. The main clay type in these rocks is kaolinite which is a much more stable clay than illite. Sample plugs were Soxhlet cleaned then pressure saturated in brine before testing. Sample plugs were normal to bedding (i.e. geological layering).

5.2 Effective Stress Conditions

The effective stress conditions applied during laboratory testing are important in establishing accurate and relevant values of Cz. The uniaxial strain compaction test conditions were chosen to as closely as possible reflect the in-situ reservoir stress conditions so that the resulting values of Cz obtained during the simulation depletion stage of the experiment as closely as possible reflect the actual reservoir compaction.

Net axial stress conditions were chosen to replicate NOBP (net overburden pressure) which exists on the samples under in-situ reservoir stress conditions. NOBP consists of pore pressure and overburden stress (vertical stress) which were estimated as follows:

- Pore Pressure was measured directly in the reservoir using wireline formation interval tests (e.g. MDTs) which are considered to be highly accurate.

- Overburden stress is considered the easiest principal stress to estimate accurately. Estimates are obtained by integrating the wireline density log. Where no density log exists, density is estimated from velocity data (e.g. VSP, checkshot, acoustic log) using empirical calibrations. Overburden stress estimates for Calliance and Torosa wells are considered particularly robust given the good density log coverage and the availability of shallow density measurements from geotechnical wells (i.e. there was little reliance on empirical methods to fill gaps in the measured density profile). An independent external review of Woodside Browse geomechanics model conducted in 2010 concluded that “The methods used to estimate the vertical stress gradient are reliable and the results calculated by JRS are consistent with those calculated by Woodside” (JRS Petroleum Research, 2010).

There is little or no scope for the calculations of in-situ vertical stress conditions to be incorrect in such a way that would make a meaningful difference to experimentally derived Cz values used to constrain compaction and subsidence at Torosa.

Different net axial stress was applied to Torosa and Calliance core samples during lab tests because of differences in reservoir depth and water depth; and thus differences in the estimated in-situ stress conditions. These differences between the wells are easier to compare when the stresses are expressed as gradients normalised for depth (Table 2; Figure 4). Pore pressure is consistent across each field and is as measured using accurate MDT measurements. The difference between Calliance-3 and Torosa-1 axial stress is consistent with the deeper water depth, and shallower sample depth at Calliance-3 (Figure 4).

Well	TVD	Water Depth	TVD	Applied Axial Stress		Pore Pressure	
	[mSS]	[m]	[mBML]	[psi]	[SG]	[psi]	[SG]
Calliance-3	3856.34	676.8	3202.37	11168	2.03	5656	1.03
Torosa-1	4346.88	476.3	3894.48	13400	2.17	6526	1.05
Torosa-6	4443.57	44	4436.84	13400	2.12	6526	1.03

Table 2: Summary of applied axial stress and pore pressure for Cz laboratory testing. The depth reference is taken as the middle of the sampled interval in each well.

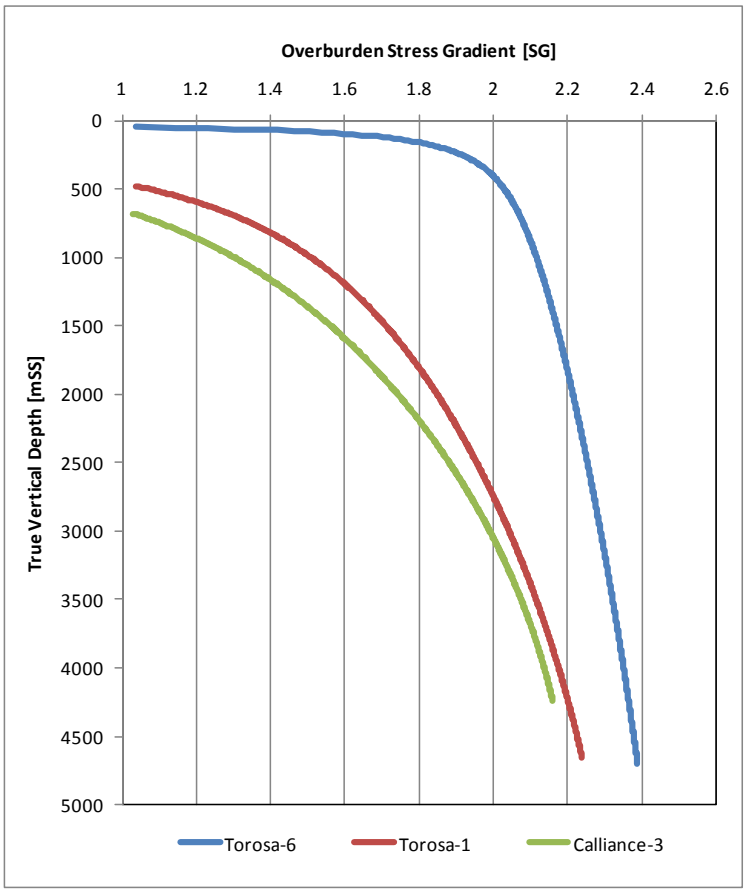

Figure 4: Overburden stress profiles for Calliance-3, Torosa-1 and Torosa-6.

Table 3 contains a comparison of current overburden stress estimates and the applied axial load used during the Cz testing program. Applied axial stress during testing was representative of the current in-situ stress estimates for Calliance-3, Torosa-6 and Torosa-1. The applied uniaxial stress is slightly lower than the in-situ stress estimates which allows for any errors in estimated overburden stress and provides for potentially conservative measurements of Cz.

Well	Applied Axial Stress during Cz testing		WEL overburden stress estimates	
	[psi]	[SG]	[psi]	[SG]
Calliance-3	11168	2.03	11647	2.12
Torosa-1	13400	2.17	13685	2.21
Torosa-6	13400	2.12	15028	2.38

Table 3: Comparison of axial stress used in Cz testing and WELs current vertical stress estimates.

The effective stress conditions at Torosa-1 are analogous to the Torosa deep-water environment (i.e. away from the reef), while the effective stress conditions at Torosa-6 are analogous to the Torosa sub-reef environment. The in-situ stress conditions at Callaince-3 are too low to be analogous to the Torosa Field.

5.3 Torosa-1

The Torosa-1 well is located in the northern section of the field and out of the core area where North Scott Reef-1, Torosa-4 and Torosa-5 are located. A total of nine Cz tests were performed by FracTech Labs, UK on plugs taken from three core barrels: six tests were carried out on J22/JP2 material and three tests on J18/JP1 material.

Torosa-1 and Torosa-6 samples were loaded to an axial stress of 200psi and radial stress of 200psi. Axial, radial and pore pressure were simultaneously ramped until pore pressure reached 6526 psi. Pore pressure was held constant while the axial and radial stress was further increased to 11,330 psi (bulk compression curve). Finally the axial stress was increased to 13,400 psi. Samples were then unloaded under uniaxial conditions. Pore pressure was decreased linearly with time from 6526 psi to ~500 psi over several hours. Radial stress was decreased during unloading, as required, to maintain zero radial strain. Reservoir depletion of ~6000 psi was simulated per instructions from Woodside to simulate end of field reservoir pressure in Torosa.

Tests were considered to be of good quality and have been used in this study. However, both Woodside and Senergy Limited (who provided local QA/QC in the UK for Woodside) considered the uniaxial strain compaction results to be high given the Torosa reservoir rocks are deeply buried, have low porosity and high measured rock strength. Rock mechanics testing conducted on Torosa-1 core by FracTech indicated very stiff rock suggesting low Cz. The stiff nature of the rocks is in agreement with the porosity and +3700 mBML depth of the reservoir as well as with visual examination of the rock.

5.3.1 J22 (JP2) sands

Six tests were conducted on the J22 (JP2) reservoir unit. The fractional volume porosity range between 6.8% to 18.7% for the J22 (JP2) samples tested. The Cz results are somewhat higher than expected given the J22 (JP2) reservoir unit is deeply buried, has low net porosity, and high measured rock strength.

5.3.2 J18 (JP1) sands

Three tests were conducted on the J18 (JP1) reservoir unit. Porosity ranges from 17.3% to 18.6% in the J18 (JP1) samples tested. The fractional volume porosity results are higher in J18 (JP1) than in J22 (JP2) as expected. The Cz results are consistent with the depth below mud line for the J22 (JP2) unit, the net porosity and rock strength test results conducted on the core material.

5.4 Torosa-6

5.4.1 J28.3 sands

Three tests were undertaken on the J28.3 reservoir unit. Testing was less extensive on the Torosa-6 core as significantly less core material was available than in Torosa-1. Testing was performed by FracTech Labs in the UK. The fractional volume porosity values are 0.5% to 16.2%. These lower numbers are not unexpected given the burial depth of the J28.3 in the lagoon area. The strain compaction results for Torosa-6 J28.3 sands, with greater burial depth in the lagoon area than the Torosa-1 J22 (JP2) and J18 (JP1) sands, are equivalent to or higher than the Torosa-1 results. This is most likely due to the better quality J28.3 sand than the Torosa-1 J22 (JP2) and J18 (JP1) sands.

5.5 Calliance-3

Four uniaxial strain compaction tests were undertaken on Calliance-3 core samples. An initial confining pressure of 580 psi was applied while increasing pore pressure to keep a constant 290 psi effective stress. Confining and pore pressure were then simultaneously increased to 5947 psi and 5656 psi respectively. Confining pressure was then further increased to 7252 psi while keeping pore pressure constant, and finally total axial stress increased to 11168 psi whilst keeping confining pressure and pore pressure constant. The sample was then considered to be under approximately in-situ stress conditions. Depletion was simulated in the final stage of each test by reducing pore pressure from 5656 psi to 725 psi under uniaxial strain conditions (i.e. altering the confining stress such that the radial strain = zero).

5.5.1 J28.4-J41 (D1)

Two tests were undertaken in the J28.4-J41 interval with porosities of 11.4% and 21.16% (Table 4).These samples have the highest measured uniaxial strain compaction coefficients consistent with the shallower burial depth at Calliance compared to Torosa. However, the uniaxial strain compaction of the sample with 11.4% porosity is anomalously high compared to the other 15 measurements.

5.5.2 J28.1-J28.3 (D2)

Two tests were undertaken in the J28.1-J28.3 (D2) interval with porosities of 9.2% and 21.64% (Table 4). The measured uniaxial strain compaction is consistent with measurements made on Torosa-1 and Torosa-6 core samples.

Well	Core depth (mMDrt)	Formation	Fractional Volume Porosity (%)	Uniaxial Strain Compaction (x10-6 bar-1)
Torosa-1	4302.29	J22 (JP2)	13.4	2.48
	4307.00	J22 (JP2)	15.2	3.30
	4319.32	J22 (JP2)	6.8	2.75
	4324.05	J22 (JP2)	14.2	3.01
	4375.57	J22 (JP2)	18.7	2.91
	4389.36	J22 (JP2)	15.7	2.68
	4395.30	J18 (JP1)	17.3	2.68
	4413.76	J18 (JP1)	17.3	2.80
	4439.26	J18 (JP1)	18.6	2.54
Torosa-6	4469.50	J28.3	14.5	3.27
	4481.89	J28.3	16.2	4.21
	4492.17	J28.3	0.5	1.72
Calliance-3	3820.67	J29.5	11.40	4.64
	3852.25	J28.4	21.16	4.34
	3906.52	J28.1	21.64	3.22
	3937.47	J28.1	9.20	2.63

Table 4: Uniaxial strain compaction coefficient from laboratory tests on samples from the Torosa-1, Torosa-6 and Calliance-3 boreholes.

5.6 Comparison to Other Fields

Uniaxial strain compaction results from the Torosa-1 and Torosa-6 boreholes fall on the lower boundary of the "well-consolidated" range classified by Shell (Figure 5), i.e. the Torosa sandstones have low Cz values for well-consolidated sandstones. The Torosa-6 plug which may have some volcanic material falls in the tight sandstone category.

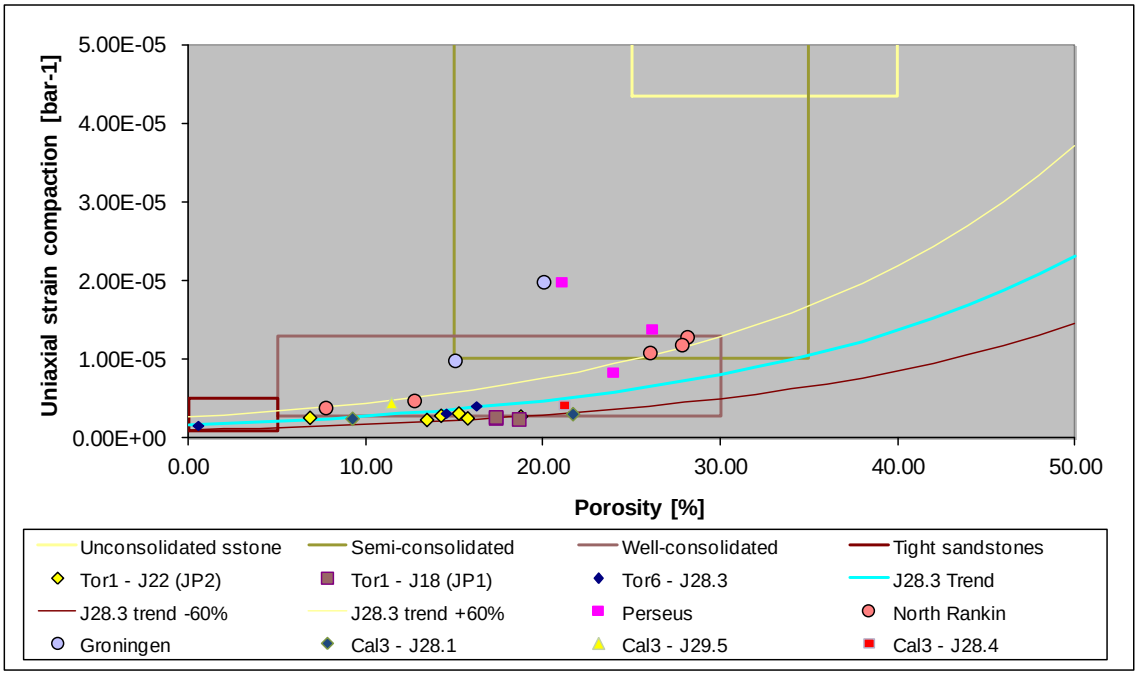

Figure 5: Uniaxial strain compaction measurements versus porosity showing Shell's classification. The porosity-compaction trends used in this study is also shown.

Sandstones from the same field under the same in-situ stress conditions can show different uniaxial strain compaction coefficients. Differences in Cz within the well-compacted range as defined by Shell are expected to be related to lithology and temperature (i.e. diagenetic effects) in addition to in-situ stress conditions. Such effects are considered to be the cause of the low Cz of the Torosa sandstones, and highlight the importance of local measurements over analogue data. Cz was measured in each of the three main reservoir intervals in Torosa (J18 (JP1), and J22 (JP2) from nine tests in Torosa-1, and J28.3 from three tests in Torosa-6) to ensure any lithological differences are captured.

The Torosa-1, Torosa-6 and Calliance-3 lab test results have been benchmarked against several analogue fields from the Carnarvon Basin where Cz data exists. Uniaxial strain compaction at Torosa is significantly less than values observed in these fields (Figure 5). However, the in-situ stress conditions at Torosa are higher than the other fields (Table 5). Indeed, the lower in-situ stress conditions at Calliance mean that Calliance is not directly analogous to Torosa. The low side outcome at Torosa was expected and is consistent with the geological setting at Torosa.

Well	True vertical depth	Water Depth	Net Overburden	Reservoir Temp

	[mSS]	[m]	Pressure [psi]	[degC]
Torosa-1*	4347	476	7159	143
Torosa-6*	4444	44	8502	147
Calliance-3*	3856	677	5992	126
North Rankin	2800	125	4725	108
Perseus	3100	128	5590	112
Groningen	2825	0	*unknown*	*unknown*

Table 5: Net overburden pressure (NOBP) at reservoir depths for fields included in Figure 6. *calculated form Table 2 & Table 3. Values for North Rankin, Perseus and Groningen are approximate only.

5.7 Porosity-Cz Relationship

A porosity-Cz relationship was fitted to the J28.3 data from Torosa using the three data points available. An exponential curve fit describes the porosity-Cz trend for the J28.3 sand where porosity (ϕ) is presented as a percentage value (Figure 6).

$$Cz\ (bar\text{-}1) = 1.657 \times 10^{-6}\ EXP \times (0.052811 * \phi)$$

The low porosity value from J28.3 sand is heavily weighted and gives an R^2 of ~0.97. Low and high-case trends were also established corresponding to the J28.3 trend ± 60% (Figure 6). An attempt was made to fit porosity-Cz trends using other data. However, no clear trend could be established from the limited number of tests in each interval. As such, the J28.3 trend is used herein. All Calliance and Torosa data including the anomalously high test from Calliance-3 fall below the high-case J28.3 trend (yellow curve in Figure 6) suggesting that the J28.3 trend is suitable to use for all sand intervals.

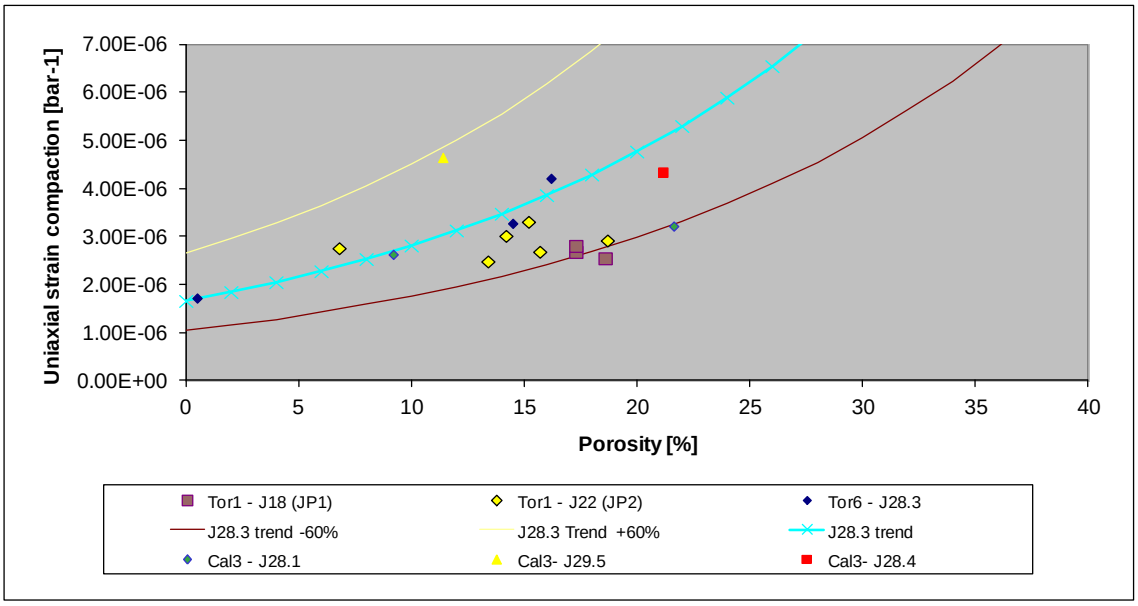

Figure 6: Porosity versus uniaxial strain compaction for all Calliance and Torosa tests.

The majority of the Torosa data fall on or below the J28.3 trendline and only one Torosa-1 J22 (JP2) sample plots slightly above the J28.3 trend (Figure 6). Therefore, it is considered that use

of the J28.3 trendline to estimate Cz at Torosa is conservative. In this context it is worth pointing out that the majority of the compaction and subsidence at Torosa is expected to result from depletion from within the deeper J18 (JP1) reservoir primarily due to the thickness and lateral extent of the J18 (JP1) reservoir. Measurements of Cz from J18 (JP1) samples fall along the J28.3 -60% trend (Figure 6).

The only measured Cz in Calliance and Torosa which falls significantly above the J28.3 trend was made on a sample from the J29.5 (D1 equivalent) in Calliance-3. The J28.4-J30 (D1 equivalent) section is largely absent in the core area of Torosa due to J40.0 (JO) erosion, however, locally this section can be preserved in the hanging walls of key faults e.g. Torosa-3. This J28.4-J30 (D1 equivalent) section at Torosa is significantly poorer quality than the equivalent section in Brecknock and Calliance, being depositionally more distal, and hence does not form a target for the Torosa development. This section tends to be volcanic prone (i.e. non-net) where it has been intersected.

The rocks at Torosa have been subjected to relatively greater in-situ stresses and are therefore expected to have lower Cz than the Calliance reservoir rocks. Therefore, that the rocks at Calliance have higher Cz values than at Torosa (the highest Cz measurements are from Calliance) was expected, and is a consistent result. The different in-situ stress conditions between Calliance and Torosa provide a reasonable basis for the exclusion of the Calliance-3 Cz results from the compaction and subsidence calculations for Torosa. However, the Calliance-3 results were included and the choice of upper and lower trend estimates for Cz was widened to ±60% to ensure the high Calliance test results fitted within the envelope (Figure 6). Interestingly, the upper bound uniaxial strain compaction trend is a good fit to the North Rankin gas field data and is therefore almost certainly an overestimate of uniaxial strain compaction in Torosa considering the differences in geological setting between Torosa and North Rankin (**Table 5**).

5.8 Pore Volume Compressibility.

Undertaking laboratory tests to determine the Cz of the specific reservoir rocks which will be subjected to depletion is a relevant and appropriate method to assess the potential for subsidence in any given field because Cz is directly related to vertical strain (εz):

$$\varepsilon z = \Delta h/h = Cz\Delta P$$

The uniaxial strain compaction testing on Torosa and Calliance core samples was designed so that the derived parameter (Cz) can be used directly to estimate compaction. However, Cz measurements are not routinely undertaken and the availability of suitable analogue data is limited.

Pore volume compressibility (Cpp), while not a direct proxy for Cz, is a related parameter which is more routinely measured and for which a larger published dataset exists. A comparison of experimentally-derived compressibility values from Torosa with industry data was conducted. The laboratory-derived pore compressibilities of Torosa rocks were compared with the worldwide data set for well-consolidated sandstones compiled by Yale et al. (1993). Their (Yale et al.) conversion formula (Cf = 0.45 Cpp) from Cpp to formation compressibility (Cf) was applied to the Torosa data to allow for a direct comparison with the worldwide data set. The range of Torosa compressibilities is consistent with the worldwide data set (over 45 formations) over the laboratory stress range that was applied to the Torosa rocks (Figure 7).

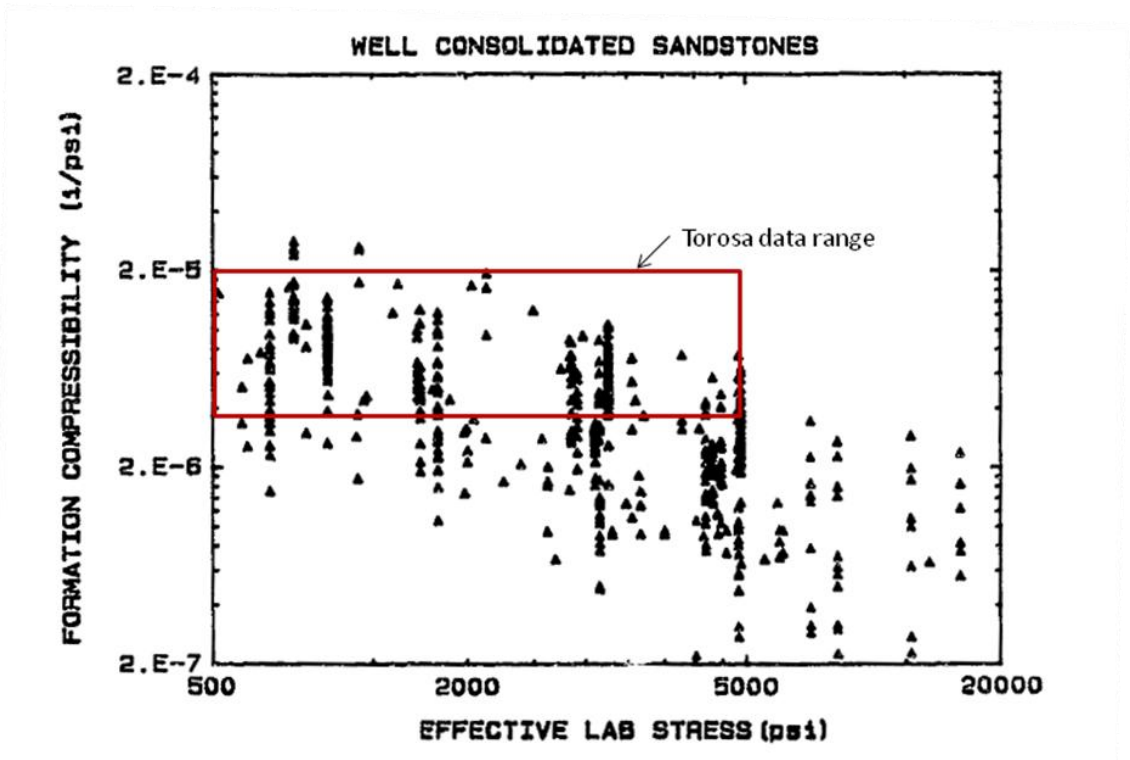

Figure 7: Comparison of the range of formation compressibilities derived for Torosa rock samples with the world-wide data set (121 samples in over 45 formations) from Yale et al. (1993) for well-consolidated sandstones. Diagram modified after Yale et al. 1993. The red box indicates the range of formation compressibilities of Torosa samples over the range of stresses that were applied in the laboratory to Torosa samples.

Note: Cpp is measured during the early loading phase of Cz tests (i.e. not measured under simulated reservoir conditions). Cpp cannot be measured under simulated reservoir conditions during Cz testing because radial strain is kept at zero during the depletion phase of the test.

6 Torosa Field Subsidence Analysis (year 2012 model)

6.1 Overview

The Torosa Field, formerly known as Scott Reef, is located approximately 300 km off of the Kimberley Coast in North West Australia. Water depth varies from <20 m to ~700 m. The field has an area of ~700 km^2 and is aligned with a long axis following a northeast-southwest trend and is approximately 50 km long by 15 km wide. The Torosa structure is similar to the nearby Brecknock Field, comprising a northeast-southwest trending Jurassic-Triassic fault block. The reservoir is an early-middle Jurassic syn-rift shallow marine/deltaic interbedded clastic sequence, the lower portion of which onlaps the Triassic structural high from the east. The structure is fault bounded to the west and dip closed to the north, south and east at the main unconformity (MU) level. Torosa is yet to reach concept select. However, all reservoir intervals in Torosa are planned to be completed with high rate gas wells to maximise off-take from the high permeability reservoir units according to the current reference case. The reservoir will be completed across multiple intervals where applicable.

The Torosa gas column is some 500 m in vertical extent, and free water level varying between 4530 to 4571 mTVDss. Net cut-off is defined by permeabilities greater than 0.01 mD and porosity greater than 5%. Both the thickness cases and net cut-off are especially important as net reservoir thickness is a critical parameter when estimating compaction and subsidence.

Pressure depletion and reservoir properties are derived from the Torosa Tranche 4 Petrel and Eclipse models (2009-2010). Table 6 describes the Torosa model basis.

Torosa Tranche 4 Model	Comment
LOW	• Torosa Tranche 4 Low Case production forecast model (ED05_HLHHLHLLL_JOTR_OPT_31) • All faults assumed sealed
MID	• Torosa Tranche 4 ED Mid Case production forecast model • (EDT00_MMMMMMMMH_OPT_31) • Cross-fault communication allowed
HIGH	• High case Torosa depletion model from Torosa Tranche 4 experimental design • (ED47_LLHHHXLHH_JOTR_OPT_31_T10) • Cross-fault communication allowed

Table 6: Torosa model basis

6.1.1 J28.3

The J28.3 interval is confined to the SW of the Torosa Field, under and adjacent to north Scott Reef (Figure 8). While the interval is expected to deplete uniformly in a High-case scenario (Figure 8), compartmentalisation remains a key uncertainty, leading to a large range of predicted pressure depletion (i.e. change in pore pressure); (Table 7).

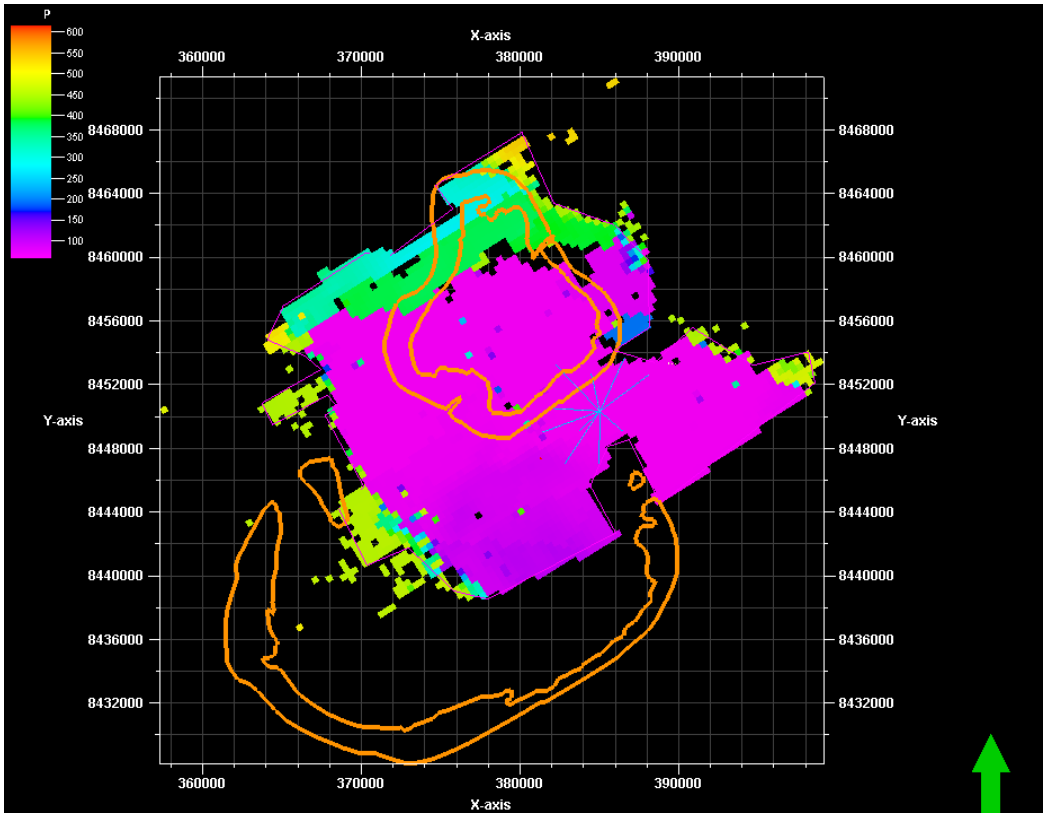

Figure 8: Expected reservoir pressure at end of field life in the J28.3 interval in the Browse Field in a high-case depletion scenario. Pressure (P) is in bar.

Variable	LOW	MED	HIGH	PDF Type	Comments
Compaction					
Porosity [%]	14	14.8	15.9	Uniform	Average from reservoir model – pore volume weighted
Compaction Coefficient [bar-1]	Trend -60%	From porosity trend	Trend +60%	Uniform	Porosity versus compaction trend
Gross reservoir height (NTG 68%) [m]	24	30	36	Uniform	Average from reservoir model
Change in pore pressure [MPa]	3.2	12.7	31.1	Uniform	Reservoir model – extreme high and low case considered
Subsidence					
Poisson's Ratio	0.22	0.28	0.36	Uniform	From log data
Radius of reservoir [km]		12.63			From reservoir model – area of disk equal to area of depleted reservoir.

Table 7: Summary of input parameters for the J28.3 interval in the Torosa Field.

6.1.2 J22 (JP2)

The J22 (JP2) reservoir interval in Torosa is confined to the Northeast of the field in the vicinity of Torosa-1 appraisal well, and is of variable quality (Figure 9).

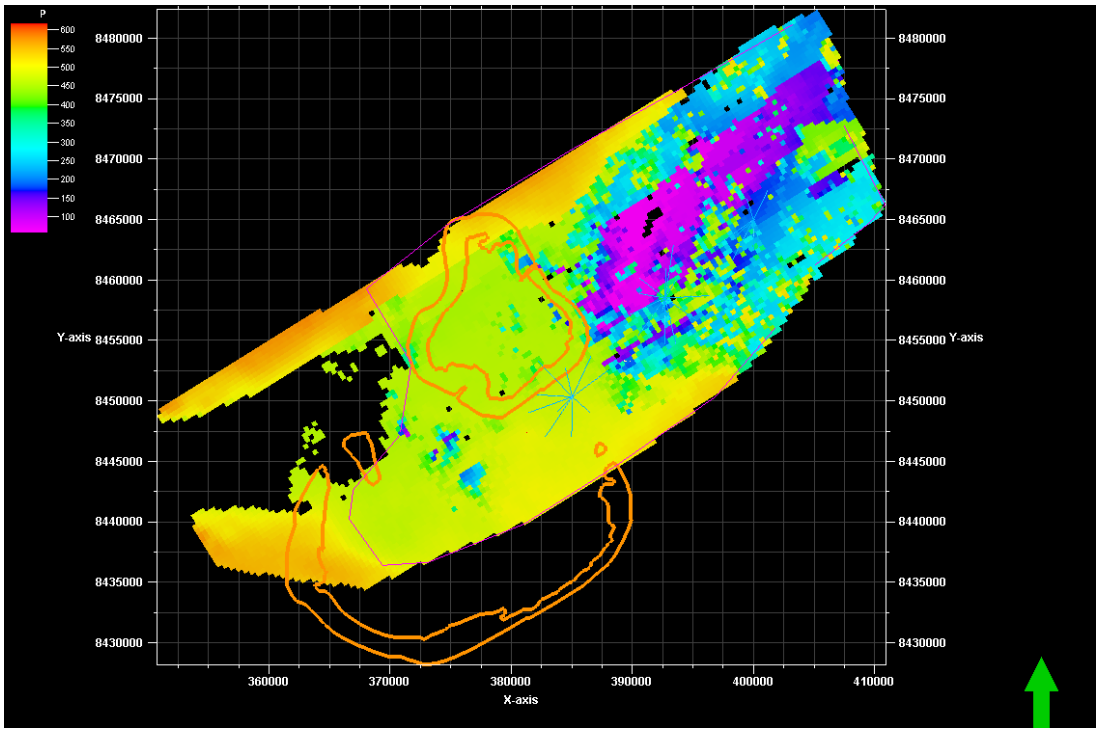

Figure 9: Expected reservoir pressure at end of field life for the J22 (JP2) production interval in the Torosa Field in a high-case depletion scenario. Pressure (P) is in bar.

Variable	LOW	MED	HIGH	PDF Type	Comments
Compaction					
Porosity [%]	11.6	12.3	13.4	Uniform	Average from reservoir model – pore volume weighted
Compaction Coeff. [MPa-1]	-60% trend	From trend	+60% trend	Uniform	Porosity versus compaction trend
Gross reservoir height (NTG 54%) [m]	27	31	36	Uniform	Average from reservoir model
Change in pore pressure [MPa]	1.1	3.0	14.7	Uniform	Reservoir model – extreme high and low case considered
Subsidence					
Poisson's Ratio	0.22	0.28	0.36	Uniform	From log data
Radius of reservoir [km]		17.95			From reservoir model – area of disk equal to area of depleted reservoir

Table 8: Summary of input variables for the J22 (JP2) reservoir interval in the Torosa Field.

6.1.3 J18 (JP1)

The J18 (JP1) sand is more widely distributed across Torosa, and demonstrates on-lapping and infilling the lows between fault blocks. Subsidence in the Torosa Field is expected to be most influenced by compaction in the J18 (JP1) interval. Pressure depletion within the J18 is also subject to uncertainty regarding fault compartmentalisation, particularly under north Scott Reef (Figure **10**). The high depletion scenario (open faults) demonstrates widespread, significant depletion throughout the J18 (JP1) interval due to production from drill centres in the open water (Figure **10**).

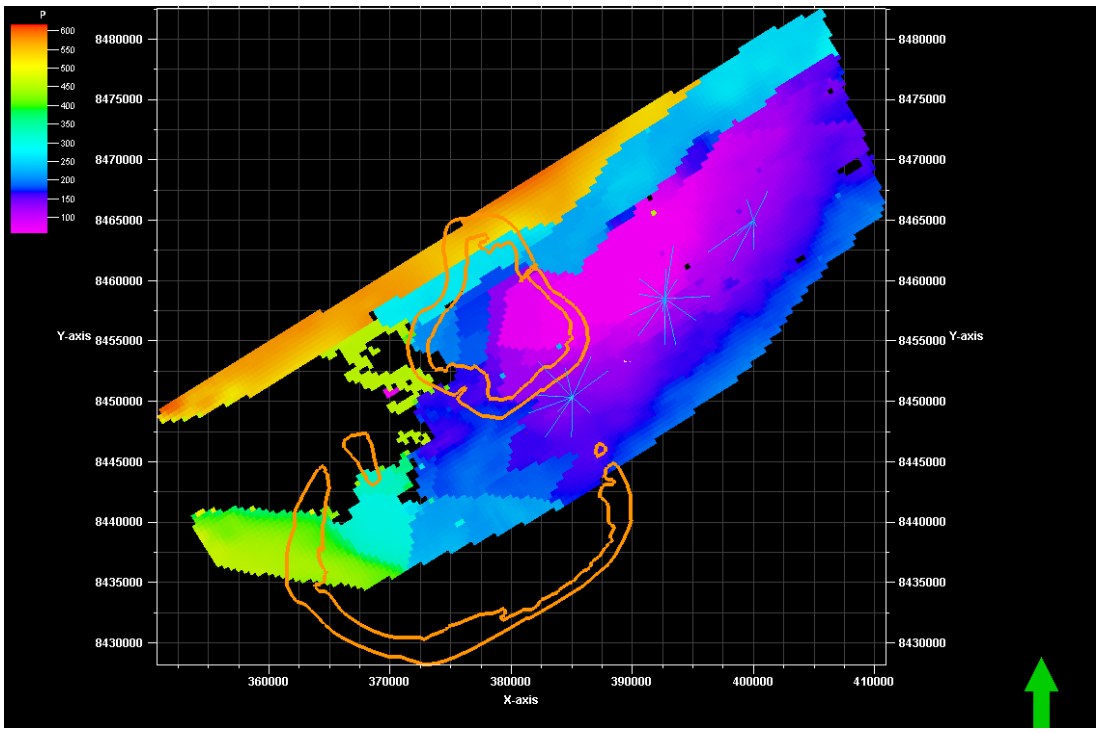

Figure 10: Expected reservoir pressure at the end of field life in the J18 (JP1) interval in the Torosa Field in a high-case depletion scenario. Pressure (P) is in bar.

Variable	LOW	MED	HIGH	PDF Type	Comments
Compaction					
Porosity [%]	9.4	11.1	12.2	Uniform	Average from reservoir model – pore volume weighted
Compaction Coeff. [MPa-1]	-60% trend	From trend	+60% trend	Uniform	Porosity versus compaction trend
Gross reservoir height (NTG 57%) [m]	75	88	102	Uniform	Average from reservoir model
Change in pore pressure [MPa]	3.6	8.6	25.6	Uniform	Reservoir model – extreme high and low case considered
Subsidence					
Poisson's Ratio	0.22	0.28	0.36	Uniform	From log data
Radius of reservoir [km]		17.95			From reservoir model – area of disk equal to area of depleted reservoir

Table 9: Summary of input parameters for the J18 (JP1) interval in the Torosa Field.

6.1.4 Other Production / Non-Net

Significant production is not expected from other intervals.

6.2 Surface Subsidence Estimates

The input parameters used for each of the producing intervals are detailed in Table 7, Table 8 and Table 9. Table 10 contains a summary of the surface subsidence estimates.

Subsidence Method	Low	Expected	High
Geertsma (1973)	2.13	4.41	7.13
Bruno (1992)	2.12	4.45	7.13

Table 10: Maximum (i.e. at the centre of the subsidence bowl) surface subsidence estimates.

6.2.1 Geertsma Method

The maximum surface subsidence (i.e. at the centre of the subsidence bowl) estimated using the Geertsma (1973) method is 4.41 cm, with 90% of model outcomes between 2.13 cm and 7.13 cm (Figure 11). Sensitivity analysis to determine the influence of uncertainty in key parameters was undertaken using a Monte Carlo simulation. Uncertainty in pore pressure change in the J18 (JP1) has the greatest influence on subsidence estimates (Figure 12). The compaction coefficient of the J18 (JP1) interval, and the pore pressure change in the J28.3 interval have a moderate influence over the subsidence estimates (Figure 12). Uncertainties in the other variables have relatively less influence on the subsidence estimates.

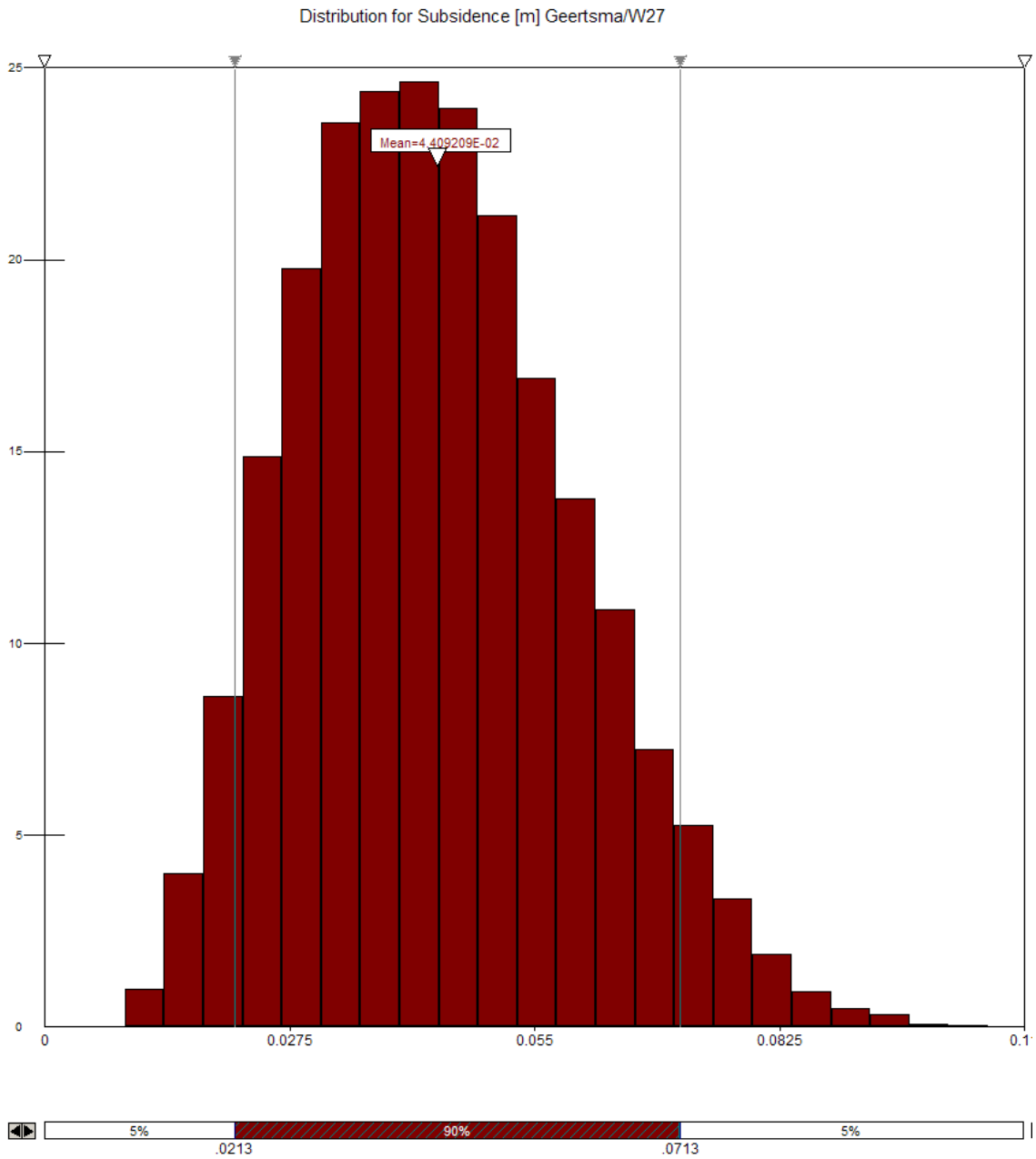

Figure 11: Maximum predicted surface subsidence for the Torosa Field estimated using the Geertsma (1973) method.

The geographical location of the centre of the subsidence bowl is subjective and has not been defined given the disk-shaped reservoir assumed in this study. A profile of subsidence as a function of distance from the theoretical centre of the subsidence bowl suggests that maximum subsidence is expected to occur up to 8 km from the centre of the subsidence bowl, and little subsidence is expected > 20 km away (Figure 13). The weighted average reservoir radius of the three producing reservoir intervals is 16.7 km. Therefore, subsidence will reduce towards the edge of the field but extend beyond the geographical extent of the field. Horizontal displacement is expected to peak at ~3 cm about 10 km away from the centre of the subsidence bowl (Figure 13). Both vertical and horizontal displacements are expected to vary smoothly away from the centre of the subsidence bowl with gentle, kilometre scale changes in displacement magnitude.

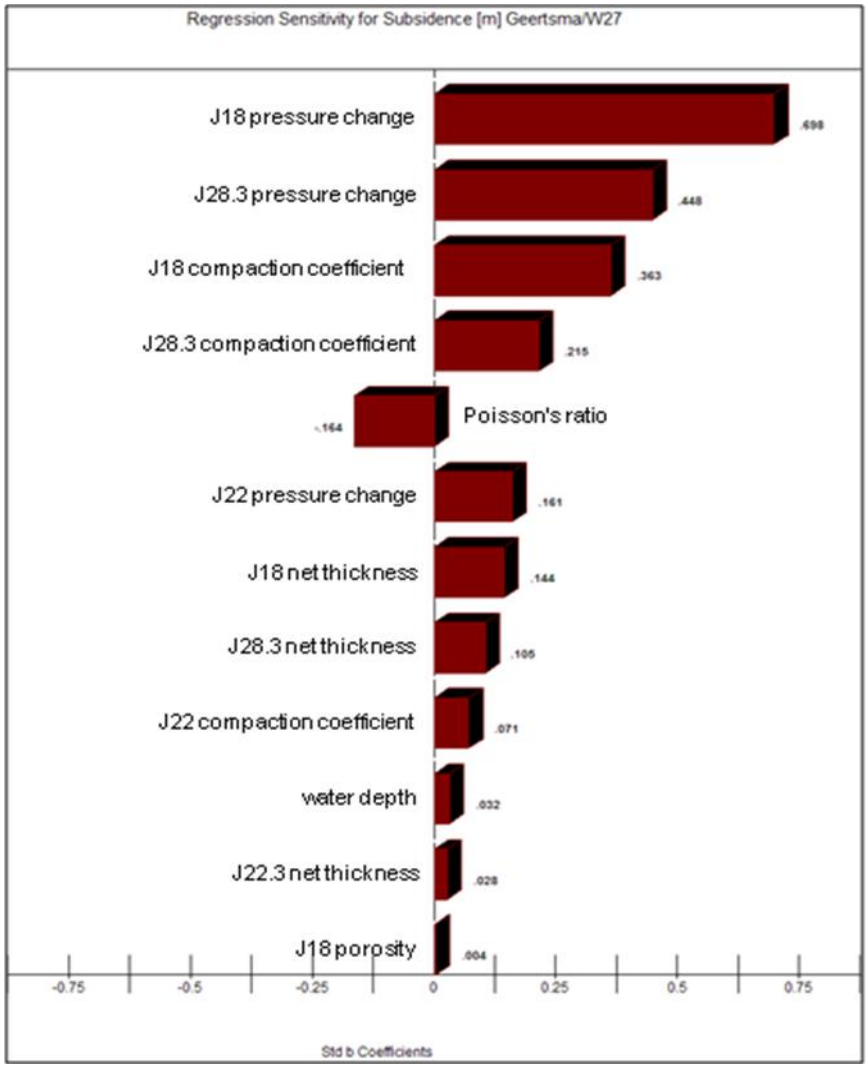

Figure 12: Tornado chart showing influence of input parameters to surface subsidence estimates for the Torosa Field calculated using the Geertsma (1973) method.

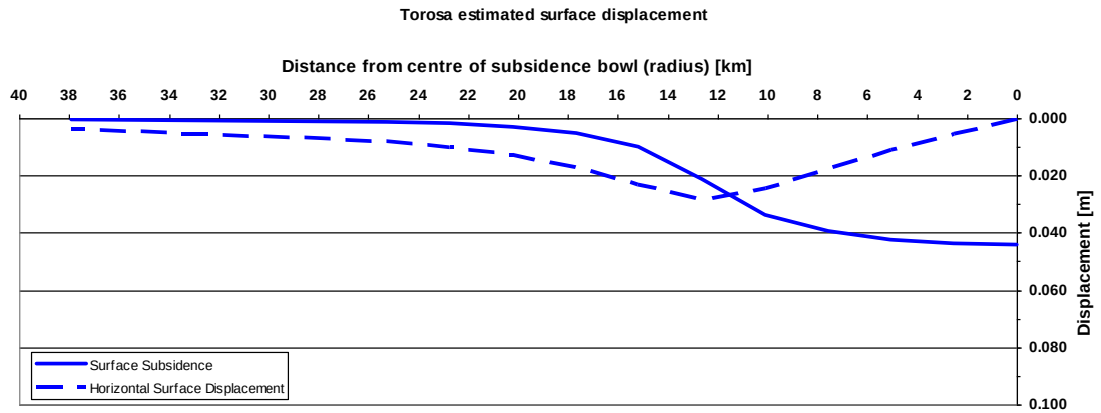

Figure 13: Surface subsidence and horizontal surface displacement profile for the expected case in the Torosa Field. Weighted average radius of the three reservoir intervals is 16.7 km. The centre of the subsidence bowl has not been interpreted as part of the study.

6.2.2 Bruno Method

Surface subsidence was also estimated using the Bruno (1992) method. Average subsidence is estimated to be 4.45 cm using the Bruno (1992) method, with 90% of model simulations between 2.12 cm and 7.13 cm (Figure 14). This is consistent with subsidence estimates generated using the Geertsma (1973) method.

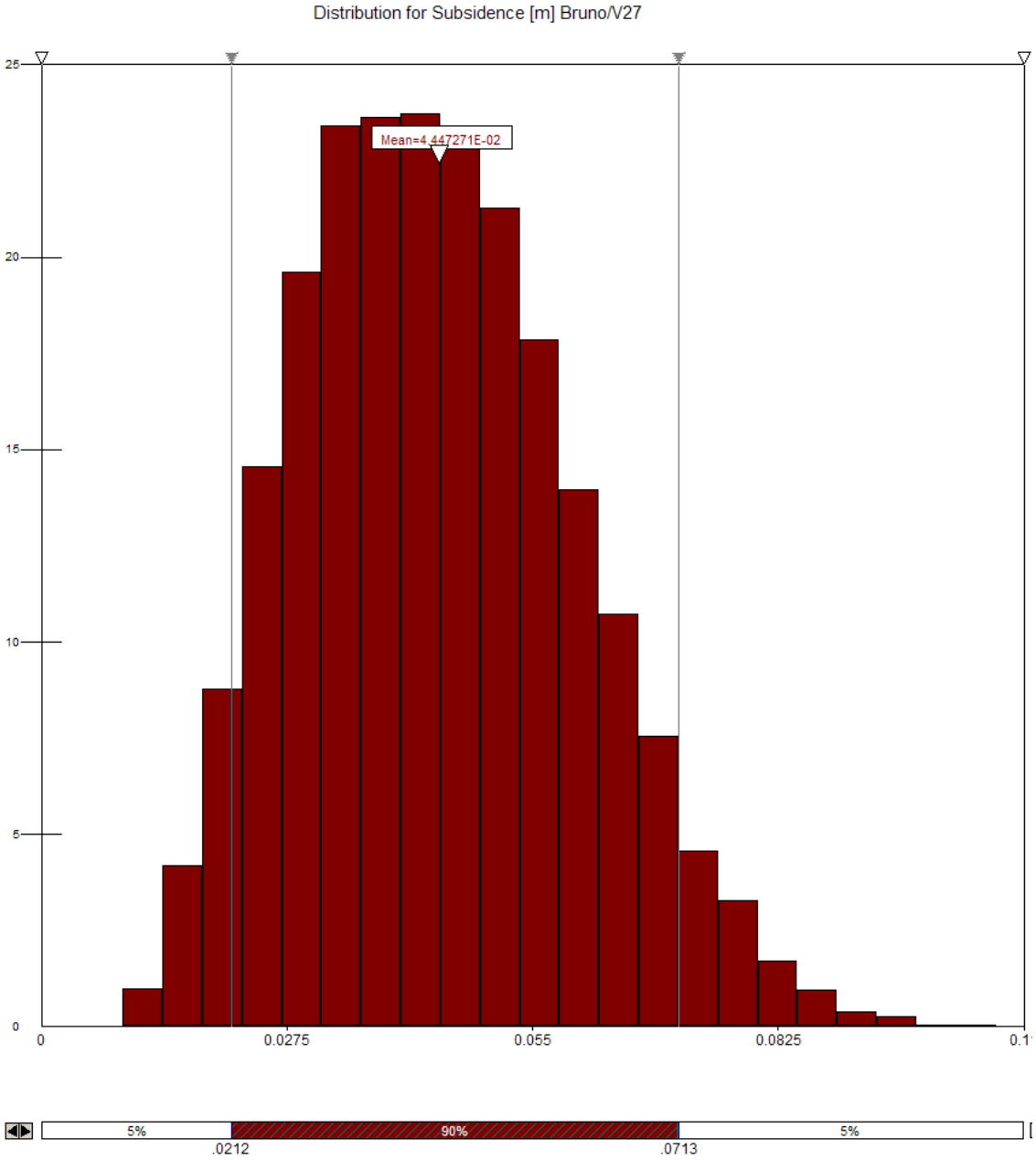

Figure 14: Maximum expected surface subsidence at end of field life for the Torosa Field calculated using the Bruno (1992) method.

6.3 Aquifer Support

Aquifer support is not expected in the Torosa Field due to down-dip reservoir quality degradation and faulting. A fully hydrodynamically connected reservoir system providing aquifer support may lead to less pressure depletion and therefore less compaction. However, such a scenario is considered unlikely and was not included in the compaction and subsidence work. While is it possible that the stepped gas-water contacts observed in the Torosa field may be due to a tilted, hydrodynamically connected reservoir system, this has not been adopted in any of

the Torosa production forecast models due to its overly-optimistic implicit cross-field connectedness and gas column height. It is more likely that fault seal or baffling over a regional scale is controlling the stepped gas-water contacts given the highly faulted nature of the structure, and gas column heights exceeding 400 m. Aquifer recharge and reservoir pressure support over a production time-scale is reduced under this scenario.

6.4 Discussion

6.4.1 Uncertainty Analysis

Uncertainty analysis using Monte Carlo simulation highlighted uncertainty in the amount of pressure depletion during production as having the largest impact on the subsidence estimates. The wide range of input depletion scenarios corresponds to uncertainty in key parameters such as intra-reservoir fault seals and aquifer support.

Uncertainty regarding fault seal and hence compartmentalisation remains a key uncertainty due to the faulted nature of the Torosa structure, and will remain that way at least until dynamic production data is obtained. In addition, drill step-out limitations associated with wellbore stability concerns, and drill-centre anchor constraints due to the presence of the north and south reefs of Scott Reef, place restrictions upon access to fault blocks, particularly immediately adjacent to and under north Scott Reef. It is therefore likely that in a high compartmentalised reservoir scenario, the level of depletion in the vicinity of north Scott Reef will be lower than in other, more easily accessible parts of the field.

The degree of compartmentalisation was a key feature differentiating the reservoir depletion models employed for the reservoir compaction work. The Low-Case model assumed all faults were sealed throughout the field, therefore significantly reducing depletion under north Scott Reef. In contrast, the High-Case depletion models assumed no additional flow barriers across faults, leading to high depletion across the field, including under north Scott Reef. However, it should be noted, for completeness, that all cases assumed some compartmentalisation over a regional scale (10-20 km) which defined free-water levels consistent with observations at appraisal wells.

Reservoir depletion values from the Low-Case and High-Case were used to estimate compaction and subsidence. Therefore, the range of compaction and subsidence estimates reflects current understanding regarding the range of possible compartmentalisation scenarios.

Uncertainty analysis also suggested uniaxial strain compaction coefficient (Cz) as having significant impact on the subsidence estimates (Figure 12). This is partly due to the conservative approach used to define a wide range of input Cz values from the experimentally-derived Cz data. The Geertsma method uses average Cz (rather than Cz from discrete samples measured in the laboratory). However, the upper-bound porosity-Cz relationship is far in excess of any single Cz measurement from the Torosa Field (Figure 6). Further uncertainty in Cz is captured by using a range of porosity estimates to calculate Cz from the porosity-Cz relationships. For example, the high case average porosity for the J28.3 interval in Torosa of 15.9 % has an associated high-case uniaxial compaction coefficient of 5.76E-06 bar-1. As such a Monte Carlo simulation run where high-case porosity and high-case uniaxial strain compaction were randomly selected would use an *average* uniaxial strain compaction significantly higher than any single value measured in the laboratory on Torosa core samples (the highest being 4.21E-06 bar-1 in Torosa-6), and twice the average of experimentally-derived Cz measurements in Torosa of 2.9E-06 bar-1. Such an approach was adopted herein in an attempt to ensure the range of predicted subsidence values cover worst-case subsidence outcomes even in the unlikely event they occur. A similarly conservative approach was used in selecting dynamic model scenarios to predict pressure depletion, porosity and net reservoir height. As such, the distributions produced by the Monte Carlo simulation are considered to contain cases with combinations of unlikely worst-case parameters leading to unrealistically high subsidence estimates.

6.4.2 Reservoir Geometry

The reservoirs at Torosa do not completely overly each other. The J18 (JP1) is extensive across the field. However, the J28.3 occurs mainly in the SW of the field while the J22 (JP2) occurs mainly in the NE of the field. Compaction and subsidence will be greater where reservoirs overlap (i.e. where cumulative reservoir thickness is greatest) as subsidence is calculated from the cumulative compaction. A worst-case scenario where all three reservoirs at Torosa were assumed to overly each other and the compaction from each of the three reservoirs was summed to get a total compaction value. Subsidence was calculated from this total compaction value. This approach maximised the contribution of each reservoir to the overall subsidence estimates. The predicted subsidence values would reduce if the geographical location of the reservoirs was considered.

The subsidence bowl is the surface expression of compaction and subsidence and differences at reservoir level will be smoothed out by the overlying rock mass. Doornhof et al (2006) note that: “A subsidence bowl tends to be approximately symmetric, even if the compaction in the underlying volume is not. Because the bowl is a superposition of subsidence resulting from each compacting element, it tends to average out the variation”. The smoothing of the compaction bowl by the rock mass overlying the reservoir will occur more for deep reservoirs like Torosa which have a thick overburden.

The geographical location of the centre of the subsidence bowl is subjective and has not been defined given the disk-shaped reservoir assumed in this study. Instead, a worst-case scenario was assumed where maximum subsidence could occur everywhere within the field and in areas surrounding the field. Therefore, the predicted values of subsidence at Torosa are not sensitive to the location of the centre of the subsidence bowl.

6.4.3 Comparison with Groningen Field, Netherlands

Subsidence has been extensively measured above the Groningen Field in the Netherlands. A maximum 24.5 cm of subsidence had occurred above the Groningen Field until 2003 (Figure 2) over a timeframe of 40 years. The predicted subsidence due to planned production at Torosa is less than measured at Groningen which is consistent with Groningen having:

- a higher uniaxial strain compaction coefficient (Figure 5);
- similar expected pore pressure decline (~3200 psi at Groningen; Ketelaar, 2009), and;
- larger net reservoir thickness (170 m in Groningen; Ketelaar, 2009).

In particular, higher Cz at Groningen implies that the subsidence at Torosa should be less than that observed at Groningen. This higher Cz at Groningen is consistent with shallower burial depth (~2825 m at Groningen compared to ~4400 m at Torosa; **Table 5**).

7 Torosa Field Subsidence Update (year 2013)

7.1 Overview

An update of the Torosa compaction and subsidence analysis was completed in 2013 capturing the output from the latest Torosa Field geological and reservoir simulation modelling (Tranche 5, 2011). The key changes between the previous model and the 2013 model update relate to:

- Updated seismic interpretation based on a single integrated velocity model, covering the Torosa-@ (Pre-SDM), Maxima 3D (Pre-SDM) and Gigas 2D (Pre-SDM) data sets
- Improved seismic resolution of faults under and adjacent to north Scott Reef
- Improved recovery of hydrocarbons from under north Scott Reef due to more sophisticated fault modelling
- Updated drainage plan (increased well count)

The improved recovery factor associated with the Tranche 5 Torosa modelling generally increased pressure depletion, resulting in more compaction and subsidence.

Changes in input parameters are described below. No changes were made to the methodology or assumptions used to estimate compaction and subsidence. Further updates may occur as the understanding of the subsurface at Torosa improves with new data (e.g. seismic data) and interpretation and with dynamic (production) data once production starts.

Pressure depletion and reservoir properties are derived from the Torosa Tranche 5 Petrel and Eclipse models (2011-2012). Table 11 describes the basis of the models used for the updated Torosa compaction analysis.

Torosa Tranche 5 Model	Comment
LOW	• Torosa Tranche 5 Low Case (P90) production forecast model • All faults assumed sealed
MID	• Torosa Tranche 5 Mid Case (P50) production forecast model • Cross-fault communication allowed
HIGH	• Torosa high case experimental design model BT02 • Very high case production outcome, not used directly for production forecasting • Cross-fault communication allowed

Table 11: Torosa updated model basis

7.1.1 J28.3

The updated input parameters for the J28.3 reservoir are contained in Table 12. The distribution of the J28.3 interval has been elongated (Figure 15). However, the changes made to the J28.3 input values from the previous modelling (see Table 7) will not have a significant influence on the compaction and subsidence estimates.

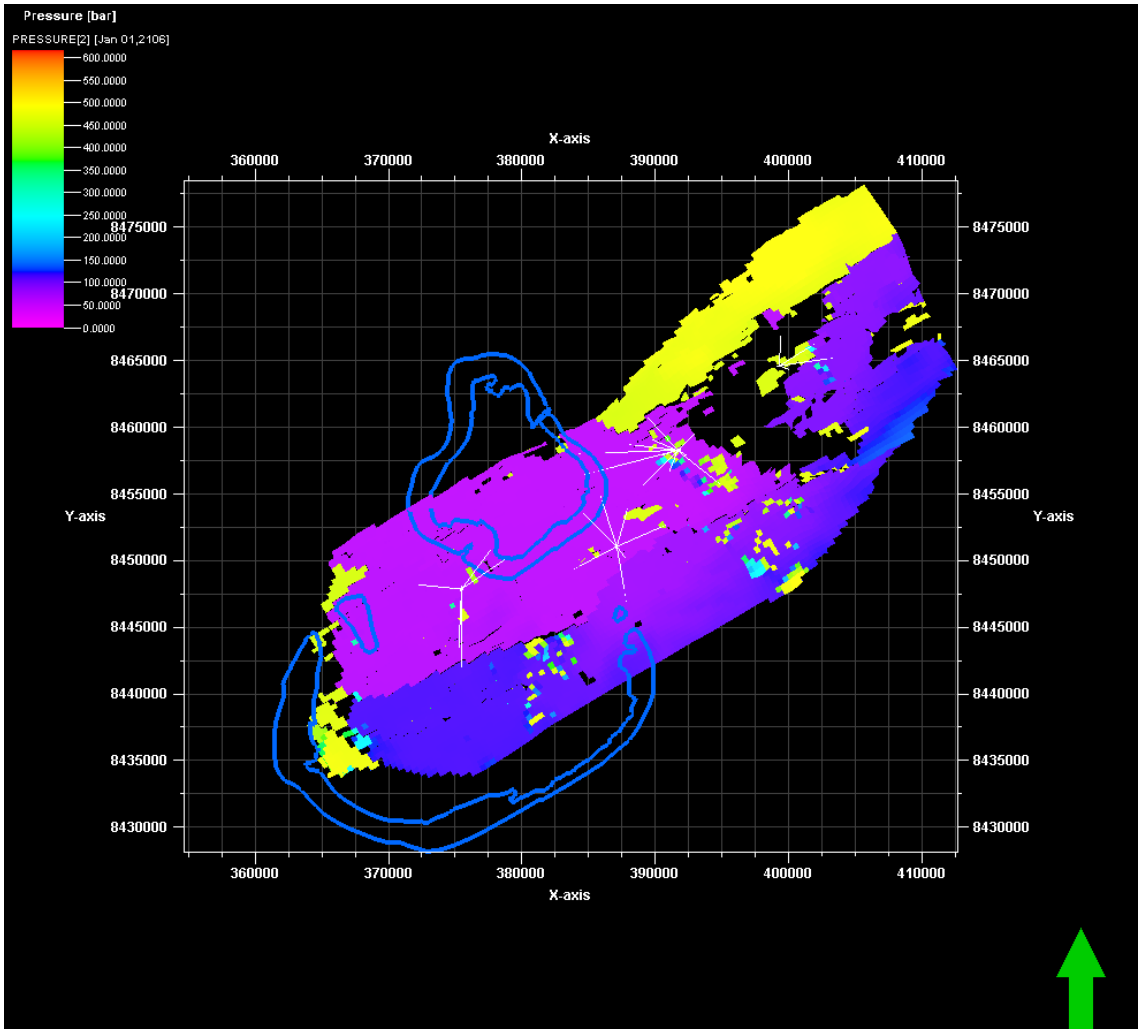

Figure 15: Expected reservoir pressure at end of field life in the J28.3 interval in the Browse Field in a high-case depletion scenario. Pressure (P) is in bar.

Variable	LOW	MED	HIGH	PDF Type	Comments

Compaction					
Porosity [%]	13.2	13.2	16.1	Uniform	Average from reservoir model – pore volume weighted
Compaction Coefficient [bar-1]	Trend -60%	From porosity trend	Trend +60%	Uniform	Porosity versus compaction trend
Gross reservoir height (NTG 68%) [m]	24	29	33	Uniform	Average from reservoir model
Change in pore pressure [MPa]	7.1	13.9	31.5	Uniform	Reservoir model – extreme high and low case considered
Subsidence					
Poisson's Ratio	0.22	0.28	0.36	Uniform	From log data
Radius of reservoir [km]		12.37			From reservoir model – area of disk equal to area of depleted reservoir.

Table 12: Summary of input parameters for the J28.3 interval in the Torosa Field.

7.1.2 J22 (JP2)

A summary of the input parameters for the J22 (JP2) interval in the original model and the updated model can be found in Table 9 and Table 13 respectively. The high case pressure depletion in the J22 (JP2) reservoir interval is significantly higher in the updated model, which will increase the estimated compaction and subsidence. The gross rock interval is also significantly thicker (although with lower net-to-gross) which will increase the estimated compaction and subsidence.

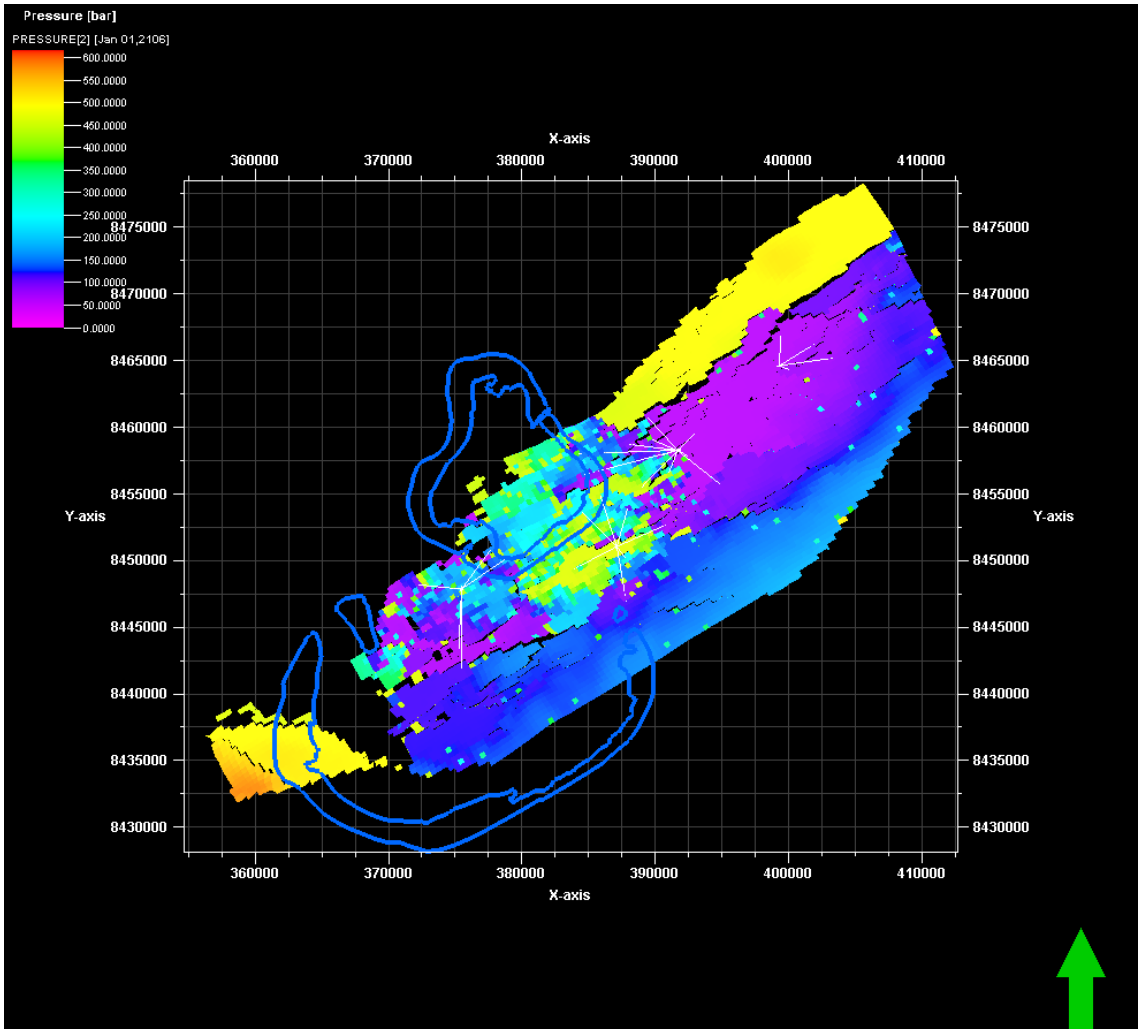

Figure 16: Expected reservoir pressure at end of field life for the J22 (JP2) production interval in the Torosa Field in a high-case case depletion scenario. Pressure (P) is in bar.

Variable	LOW	MED	HIGH	PDF Type	Comments

Compaction					
Porosity [%]	9.7	9.8	12.5	Uniform	Average from reservoir model – pore volume weighted
Compaction Coeff. [MPa-1]	-60% trend	From trend	+60% trend	Uniform	Porosity versus compaction trend
Gross reservoir height (NTG 32%) [m]	72	75	77	Uniform	Average from reservoir model
Change in pore pressure [MPa]	0.5	3.9	26.6	Uniform	Reservoir model – extreme high and low case considered
Subsidence					
Poisson's Ratio	0.22	0.28	0.36	Uniform	From log data
Radius of reservoir [km]		16.70			From reservoir model – area of disk equal to area of depleted reservoir

Table 13: Summary of input variables for the J22 (JP2) reservoir interval in the Torosa Field.

7.1.3 J18 (JP1)

The distribution of the J18 (JP1) interval is broadly similar in the two models (Figure **10** and Figure **17**). Input data for the J18 (JP1) interval (the main reservoir interval) for the original and the update model can be found in Table 9 and Table 14 respectively. Porosity, thickness and pore pressure change are all slightly larger in the updated model which will increase the predicted compaction and subsidence.

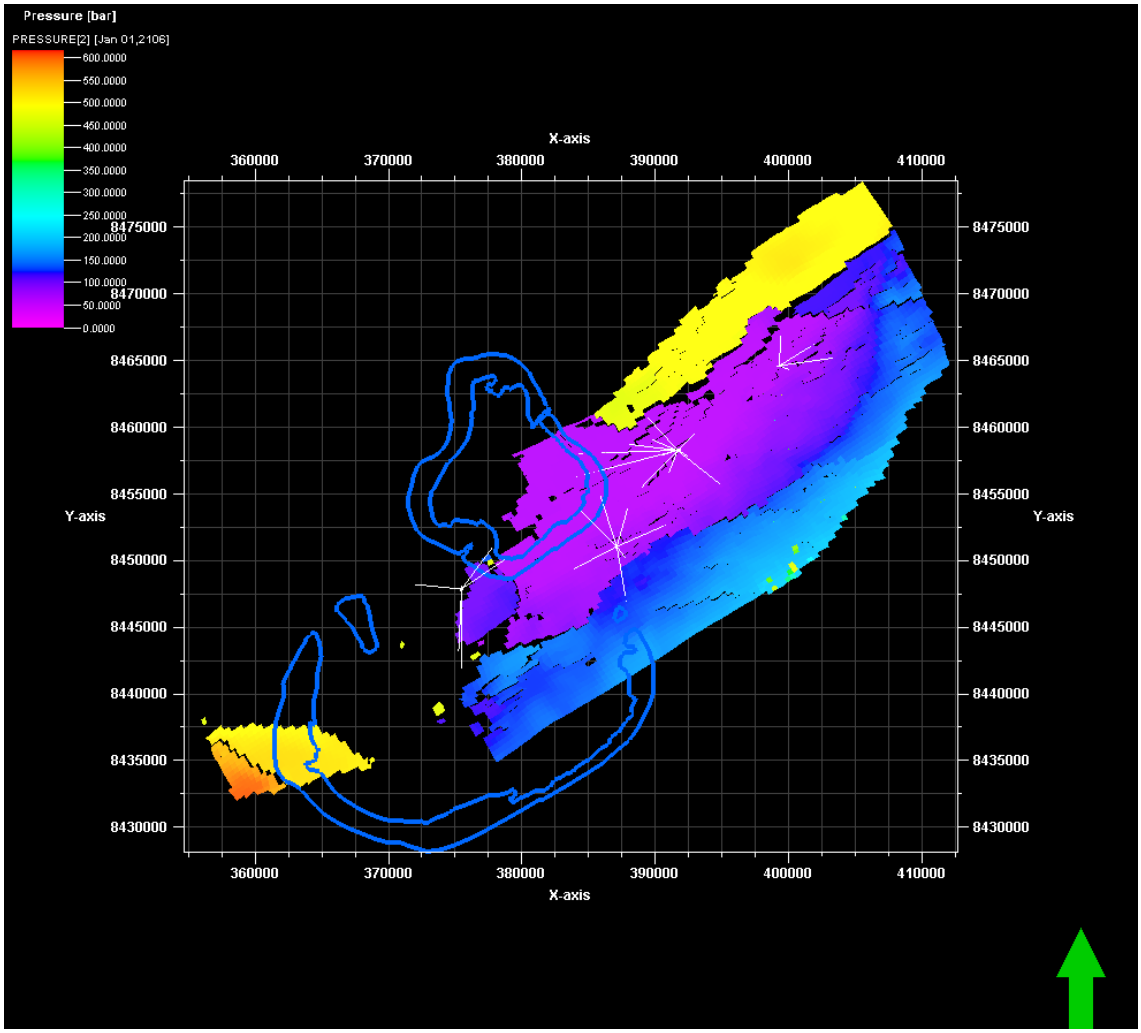

Figure 17: Expected reservoir pressure at the end of field life in the J18 (JP1) interval in the Torosa Field in a high-case depletion scenario. Pressure (P) is in bar.

Variable	LOW	MED	HIGH	PDF Type	Comments

Compaction					
Porosity [%]	10.3	10.3	12.7	Uniform	Average from reservoir model – pore volume weighted
Compaction Coeff. [MPa-1]	-60% trend	From trend	+60% trend	Uniform	Porosity versus compaction trend
Gross reservoir height (NTG 53%) [m]	103	111	124	Uniform	Average from reservoir model
Change in pore pressure [MPa]	3.3	12.2	27.1	Uniform	Reservoir model – extreme high and low case considered
Subsidence					
Poisson's Ratio	0.22	0.28	0.36	Uniform	From log data
Radius of reservoir [km]		15.75			From reservoir model – area of disk equal to area of depleted reservoir

Table 14: Summary of input parameters for the J18 (JP1) interval in the Torosa Field.

7.2 Surface Subsidence Estimates

The input parameters used for each of the producing intervals are detailed in Table 12, Table 13 and Table 14. The updated range of predicted subsidence has increased slightly to between 2.56 and 8.96 cm based on the updated model data (Table 15).

Subsidence Method	Low	Expected	High
Geertsma (1973)	2.58	5.45	8.93
Bruno (1992)	2.56	5.48	8.96

Table 15: Maximum (i.e. at the centre of the subsidence bowl) surface subsidence estimates.

7.2.1 Geertsma Method

The maximum surface subsidence (i.e. at the centre of the subsidence bowl) estimated using the Geertsma (1973) method is 5.45 cm, with 90% of model outcomes between 2.58 cm and 8.93 cm (Figure 11). Sensitivity analysis to determine the influence of uncertainty in key parameters was undertaken using a Monte Carlo simulation. Uncertainty in pore pressure change has the greatest influence on subsidence estimates (Figure 12). The compaction coefficient of the J18 (JP1) interval, and to a lesser extent the compaction coefficients of the J22 (JP2) and J28.3 intervals, have a moderate influence over the subsidence estimates (Figure 12). Uncertainties in the other variables have relatively less influence on the subsidence estimates.

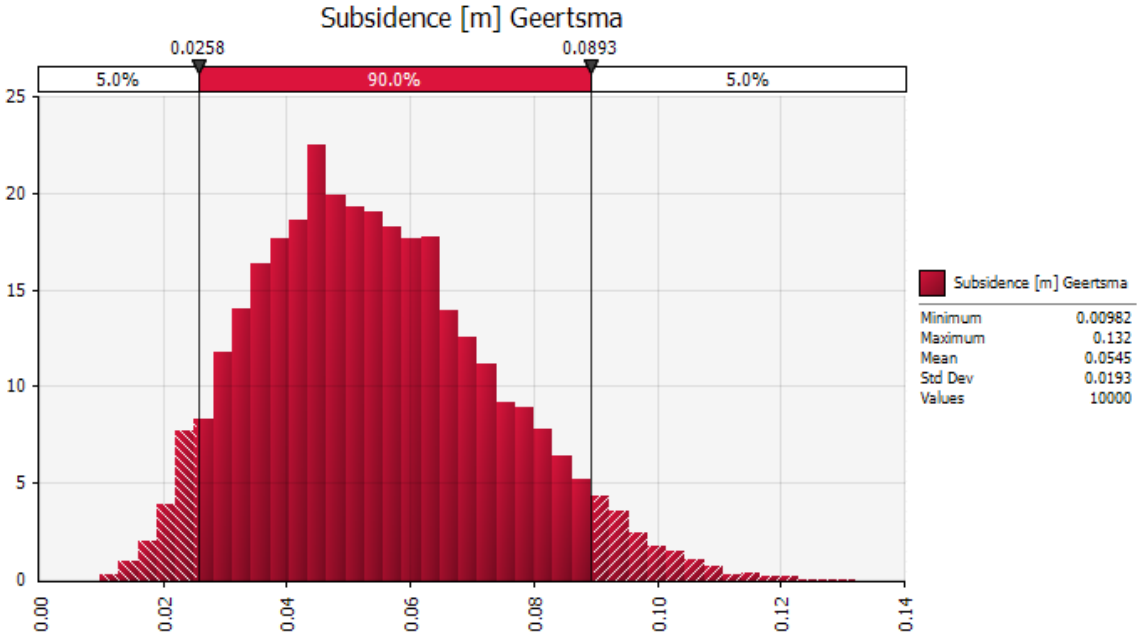

Figure 18: Maximum predicted surface subsidence for the Torosa Field estimated using the Geertsma (1973) method.

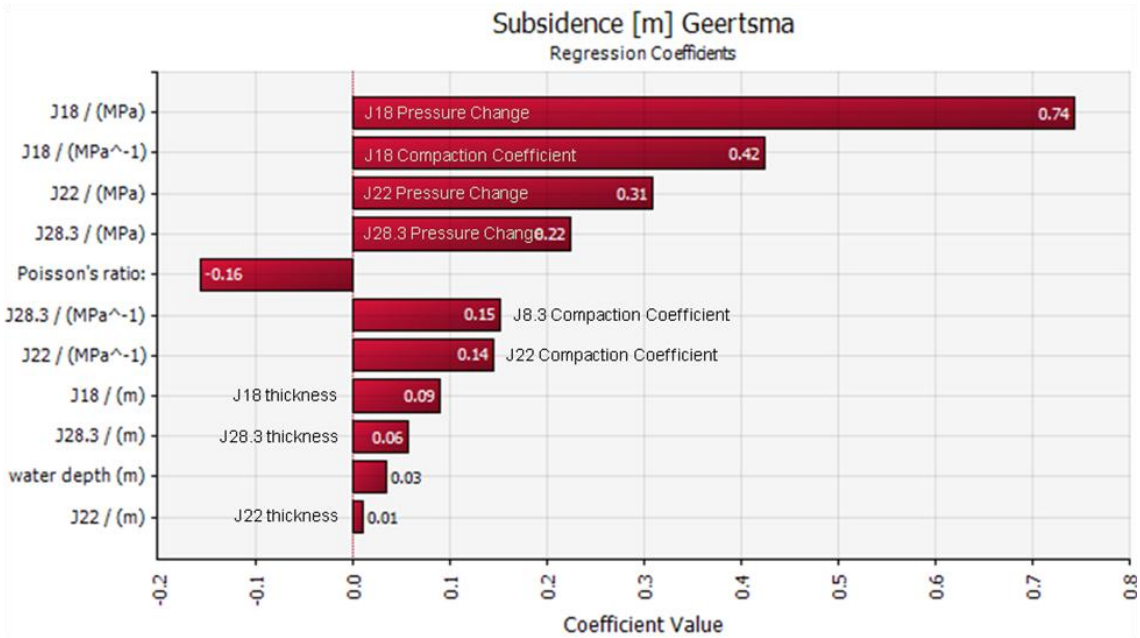

Figure 19: Tornado chart showing influence of input parameters to surface subsidence estimates for the Torosa Field calculated using the Geertsma (1973) method.

7.2.2 Bruno Method

Surface subsidence was also estimated using the Bruno (1992) method. Average subsidence is estimated to be 5.48 cm using the Bruno (1992) method, with 90% of model simulations between 2.56 cm and 8.96 cm (Figure 14). This is consistent with subsidence estimates generated using the Geertsma (1973) method.

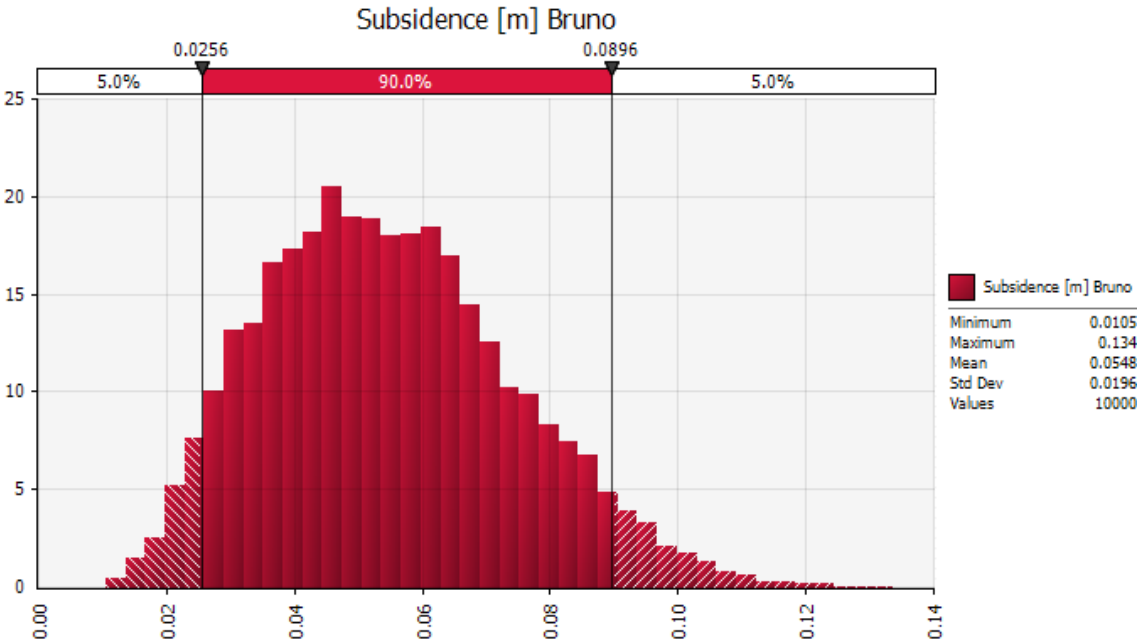

Figure 20: Maximum expected surface subsidence at end of field life for the Torosa Field calculated using the Bruno (1992) method.

8 References

Bruno, M. S. (1992). Subsidence-Induced Well Failure, *SPE Drilling Engineering*, June, 1992, pp. 148-152.

Doornhof, D., Golder Kristiansen, T., Nagel, N.B., Pattilo, P.D., and Sayers, C. (2006) Compaction and Subsidence. Oilfield Review.

Geertsma, J. (1973). Land Subsidence over Compacting Oil and Gas Reservoirs. *Journal of Petroleum Technology*, June, 734-744.

JRS Petroleum Research (2010) Browse Development Geomechanics Review.

Ketelaar, V.B.H (2009) *Satellite Radar Interferometry, Subsidence Modelling Techniques*, Springer Science, 290 pages.

Yale, D. P., G.W. Nabor and J. A. Russell. (1993). Application of variable formation compressibility for improved reservoir analysis. SPE paper #26647.